IVYSPRING INTERNATIONAL PUBLISHER

Theranostics

2019; 9(15): 4255-4264. doi: 10.7150/thno.35606

Research Paper

Dual-Channel Fluorescence Imaging of Hydrogel Degradation and Tissue Regeneration in the Brain

G. Kate Park[1,2], Su-Hwan Kim[3], Kyungmin Kim[3], Priyanka Das[2], Byung-Gee Kim[1,3,4], Satoshi Kashiwagi[2], Hak Soo Choi[2]✉, and Nathaniel S. Hwang[1,3,4]✉

1. Interdisciplinary Program in Bioengineering, Seoul National University, Seoul 151-742, South Korea
2. Gordon Center for Medical Imaging, Department of Radiology, Massachusetts General Hospital and Harvard Medical School, Boston, MA 02114, USA
3. School of Chemical and Biological Engineering, Institute of Chemical Processes, Seoul National University, Seoul 151-742, South Korea
4. Institute of Bioengineering, BioMAX Institute, Institute of Molecular Biology and Genetics, Seoul National University, Seoul 151-742, South Korea

✉ Corresponding authors: H.S.C. hchoi12@mgh.harvard.edu and N.S.H. nshwang@snu.ac.kr

Received: 2019.04.09; Accepted: 2019.05.06; Published: 2019.05.31

Abstract

The ability of brain tissue to regenerate is limited; therefore, brain diseases (i.e., trauma, stroke, tumors) often lead to irreversible motor and cognitive impairments. Therapeutic interventions using various types of injectable biomaterials have been investigated to promote endogenous neural differentiation. Despite promising results in pre-clinical studies, the translation of regenerative medicine to the clinic has many challenges due to the lack of reliable imaging systems to achieve accurate evaluation of the treatment efficacy.

Methods: In this study, we developed a dual-channel fluorescence imaging technique to simultaneously monitor tissue ingrowth and scaffold disintegration. Enzymatically crosslinked gelatin-hyaluronic acid hydrogel was labeled with 800 nm fluorophore, ZW800-3a, while the regenerated tissue was highlighted with 700 nm brain-specific contrast agent, Ox1.

Results: Using the multichannel fluorescence imaging system, tissue growth and degradation of the NIR hydrogel were simultaneously imaged in the brain of mice. Images were further analyzed and reconstructed to show both visual and quantitative information of each stage of a therapeutic period.

Conclusion: Dual-channel *in vivo* imaging systems can provide highly accurate visual and quantitative information of the brain tissue ingrowth for the evaluation of the therapeutic effect of NIR hydrogel through a simple and fast operating procedure.

Key words: NIR injectable hydrogel, Brain tissue regeneration, Multichannel imaging, Fluorescence imaging

Introduction

Brain diseases and traumatic injuries such as strokes are often incurable due to the lack of adequate medical treatment, leaving permanent tissue damage that often result in neurological disabilities [1, 2]. It was recently discovered that the brain has neurogenic progenitor cells (NPC), and its capacity for vasculature and tissue de novo formation can be promoted by providing an artificial extracellular matrix for cell infiltration and differentiation [3, 4]. Various compositions of biomaterials have therefore been investigated, including modified hydrogels, that showed promising potential for the repair of brain tissue [5, 6]. Although the therapeutic feasibility of injectable hydrogels for the treatment of brain tissue damage and stroke cavity is generally accepted, their *in vivo* behavior and contribution to brain tissue regeneration remains poorly understood [7-9].

The major challenge with neural damage treatments that utilize scaffolds is the lack of availability of tissue-specific contrast agents and *in vivo* imaging system that can provide accurate information on the efficacy and behavior of injected hydrogel on tissue ingrowth [10, 11]. A combination of fluorophore-labeled scaffold and Magnetic Resonance Imaging (MRI) has been used to achieve multimodal image analysis; however, MRI images only suggest the onset of vascularization within the scaffold [12, 13]. Spatial overlap between fluorescence

and MRI images cannot be attained to provide precise information on tissue regeneration. The current standard method used to show scaffold response to tissue growth is the *ex vivo* histological analysis of immunohistochemistry against specific antigens at the microscopic level [14, 15]. Thus, it is difficult to evaluate the overall interaction/integration with the host tissue/cells and the implanted hydrogel in a continually changing *in vivo* environment.

We hypothesized that multispectral near-infrared (NIR) fluorescence imaging could provide simultaneously monitoring of cell/tissue infiltration (NIR #1) and scaffold degradation for the optimization of the composition of scaffold (NIR #2), leading to efficient treatment outcomes. In this study, we have fabricated hydrogels composed of hyaluronic acid (HA) and gelatin to mimic the mechanical properties of native brain tissue by providing extracellular matrix support, with improved cell infiltration and proliferation. Dual-channel fluorescence imaging was performed to test the efficacy of the hydrogels by utilizing NIR brain-specific contrast agents and conjugating fluorophore to the hydrogels in 700 and 800 nm channels, respectively. In addition, we applied image segmentation analysis to the therapeutic region of the brain to provide precise visual information as well as quantitative data on the tissue ingrowth over the regeneration period.

Results and Discussion

Engineering of injectable NIR hydrogels

NIR fluorescence has many advantages for biomedical imaging, including relatively low tissue absorption, reduced scattering, and minimal autofluorescence [16-18]. We developed injectable NIR hydrogels by conjugating an 800 nm indocyanine NIR fluorophore ZW800-3a through the carboxylic functional group, which enables conjugation with an amine group in gelatin (**Figure 1A**). To avoid any adverse effects, it is crucial for the engineered hydrogel to have minimum *in vivo* protein interactions after degradation. ZW800-3a has been reported to have a low level of toxicity and fast excretion because of its charge distribution and hydrophilicity (log*D* at pH 7.4 = -1.63) [19, 20]. The physiochemical and optical properties of ZW800-3a can be found in Supplementary Information (**Figure S1-S2**).

Hydrogels composed of hyaluronic acid (HA), major components within brain ECM, and gelatin are known to provide an extracellular matrix for neural differentiation [21]. Therefore, we initially prepared tyramine-conjugated HA (HA-ty) and crosslinked with NIR-gelatin using recombinant tyrosinase isolated from Streptomyces avermitilis (SA_Ty) [22]. Our previous study has demonstrated that the SA_Ty allow ultra-fast conversion of monophenol to crosslinkable o-quinone groups in both tyramine conjugated HA and gelatin [23]. This allow tyrosinase-dependent crosslinkable and adhesive hydrogels to be formed from HA-ty. Furthermore, addition of NIR-gelatin in HA-ty allows formation of stiffer and cell-adhesive NIR hydrogel crosslinking of HA-ty and gelatin.

The schematic overview of the dual-channel monitoring of tissue growth and hydrogel behavior is shown in **Figure 1B**. The multispectral FLARE imaging system provided simultaneous acquisition of color video and two independent channels of NIR fluorescence in the range of 650-900 nm (**Figure S3**). We utilized the 800 nm channel to track NIR hydrogel behavior on 1-, 7-, 14-, and 21-d post-transplantation and the 700 nm channel for monitoring brain tissue ingrowth by the intravenous administration of Ox1 1 h prior to performing dual-channel fluorescence imaging. Oxazine derivatives with low molecular weight (<500 Da) and medium lipophilicity (log*D* 1-3) can cross intact blood-brain-barrier (BBB) and accumulates in the parenchyma of the brain [24]. We discovered that Ox1, phenoxazine structure fluorophore emitting at 700 nm, has significant uptake into the brain for detection after intravenous administration. The physiochemical and optical properties of Ox1 can be found in **Supplementary Information** (**Figure S1-S2**).

Mechanical and rheological property of NIR hydrogels

Mechanical and rheological characterization of the injectable NIR hydrogel is essential to achieve optimal therapeutic efficacy, as they play critical role on the migration, proliferation, and differentiation of neural stem cells. The stiffness of hydrogel provides the structural support within the damaged brain cavity while influencing cell invasion and phenotype of neural progenitor populations [25]. In addition, the retention of scaffold within the brain cavity and the associated host response is highly dependent on the compatibility with the implanted substrate; therefore, it should have brain-tissue-like characteristics [26].

Two different NIR hydrogels with different compositions, 1% and 3% of NIR-gelatin with fixed concentration of 1% HA, was prepared, and young's modulus (Y) was measured (**Figure 2A**). Young's modulus of 1% NIR-gelatin ranged between 3.9 to 7.3 kPa and 3% NIR-gelatin ranged between 31.2 and 49.7. We have compared the modulus of brain tissue from other studies and the reported range was

between 3 and 10 kPa [27-29]. Interestingly, numerous studies have shown that neural stem/progenitor cell proliferation and differentiation exhibited maximal potential on the soft surfaces (Y = ~ 3.5 kPa) [25], highlighted red in the graph. Areas with higher nuclear density within the brain were also reported to be softer when compared with the lower nuclear density area [30]. 1% NIR hydrogel has a better mechanical match with the brain tissue as it mimics the soft mechanical environment for neural stem cell differentiation.

Rheological property of the hydrogel is important because when injected into the defect cavity of the brain, the implant should have enough viscoelasticity to be able to hold the original injected form and continuously provide the matrix for the neural cells in the process of enzymatic degradation. The amplitude sweep test of the 1% and 3% NIR-gelatin was performed at a constant frequency of 1% to evaluate the rheological properties of the hydrogels (**Figure 2B**). The crossover of G′ and G″ for 1% and 3% NIR-gelatin was at about 80% and 150% strain, respectively. The internal structure of hydrogel broke at the crossover point of G′ and G″; beyond this point, the original structure of the NIR hydrogel was lost. Next, we measured frequency sweep to determine the dynamic behavior of the NIR hydrogel (**Figure 2C**). Compared with 1% and 3% composition of NIR-gelatin, 3% had higher storage (G′) and loss (G″) than 1% NIR-gelatin, indicating 1% NIR-gelatin is less stiff than 3% NIR-gelatin. Despite the differences in the stiffness, both 1% and 3% NIR-gelatin had high critical strain and elasticity and can withstand relatively large deformation force while only 1% NIR-gelatin exhibits the softness essential for neurogenesis.

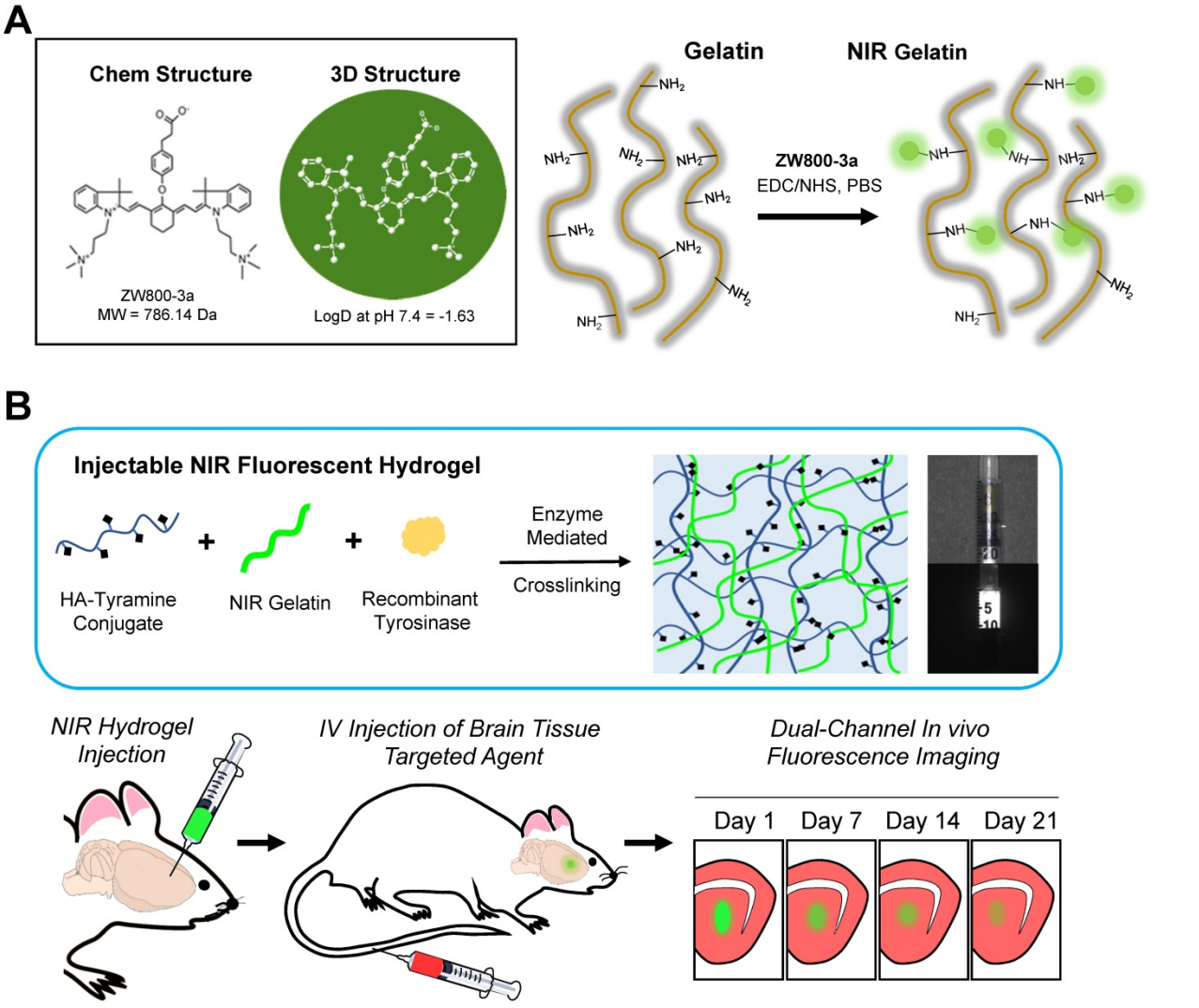

Figure 1. Dual-channel imaging of NIR hydrogel and brain tissue ingrowth. (A) Chemical structure of ZW800-3a and its chemical conjugation on gelatin. **(B)** Overall Strategy of multichannel NIR imaging for the *in vivo* assessment of tissue ingrowth and scaffold degradation. Preparation of injectable NIR hydrogel by crosslinking tyramine conjugated hyaluronic acid (HA) and NIR-gelatin with tyrosinase for the intracranial injection. Intravenous administration of Ox1 1 h prior to *in vivo* imaging of the brain. Dual-channel imaging of tissue ingrowth and hydrogel degradation under 700 nm (red color) and 800 nm channel (green color), respectively. Scale bar = 5 mm.

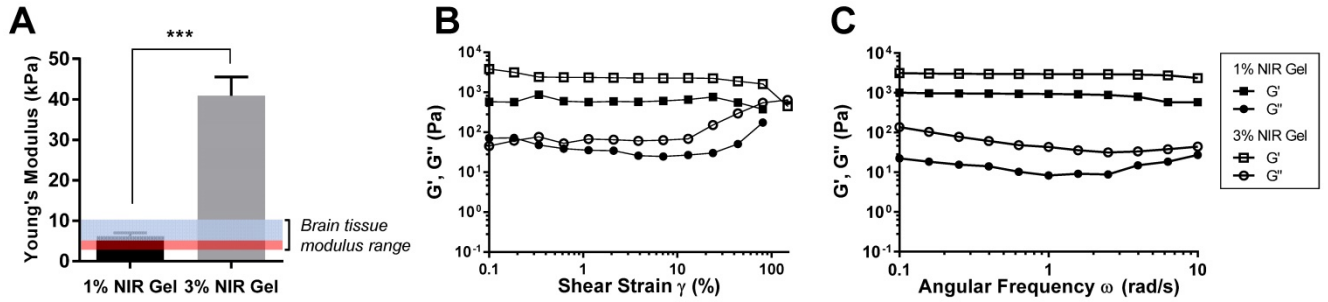

Figure 2. Mechanical and rheological evaluation of NIR hydrogel. (A) Young's Modulus of NIR hydrogel of different compositions. The highlighted blue and red region indicates range of young's modulus of brain tissue. The highlighted red region is a range of high neural proliferation and differentiation. **(B)** Amplitude sweep of NIR hydrogels. **(C)** Frequency sweep of NIR hydrogels. Data are representative of n=3 samples.

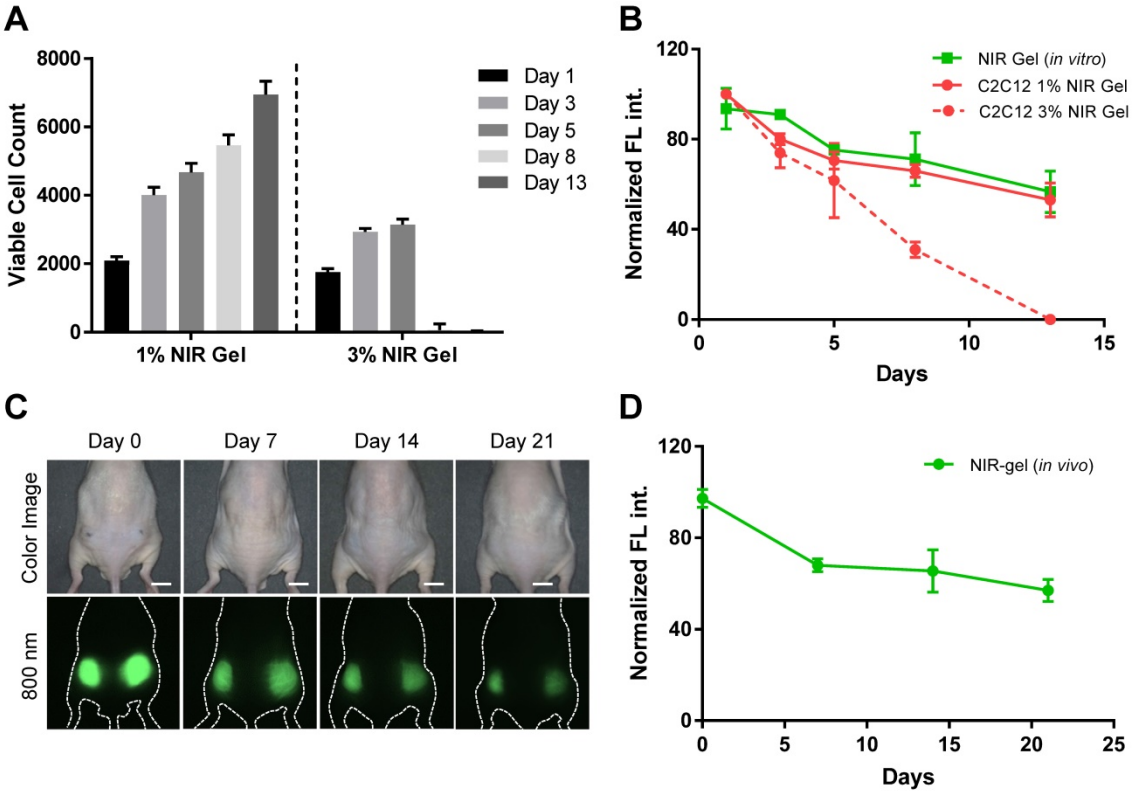

Figure 3. *In vitro* and *in vivo* viability and stability test. (A) Viability of myoblasts (C2C12) in 1 and 3 wt% of NIR-gelatin with fixed amount of HA-ty (1 wt%) for up to 2 weeks. **(B)** *In vitro* quantification of signal change of C2C12 labeled with ESNF13 (5 μM) and NIR hydrogel over the time course. NIR hydrogels in 10% FBS were used as control. **(C)** Real-time longitudinal noninvasive imaging of NIR hydrogel (100 μL) injected into the subcutaneous of nude mice for up to 3 weeks. **(D)** Quantitative plotting of the *in vivo* signal reduction of NIR hydrogel over time. Scale bars = 1 cm. Data are representative of n = 3 samples or animals.

In vitro cell viability test of NIR hydrogels

Next, we investigated *in vitro* cell viability and proliferation of C2C12 in 1% and 3% NIR-gelatin encapsulated system. C2C12 was labeled with 700 nm NIR fluorophore, ESNF13, previously reported for the use of the longitudinal cell tracking with an excellent optical property [31]. The molecular structure and optical properties of ESNF13 can be found in the supporting information (**Figure S1**). After 30 min incubation with 5 μM of ESNF13, C2C12 were detached from the Petri dish and embedded in 1 wt% or 3 wt% NIR-gelatin with a fixed concentration of HA-ty (1 wt%). Tyrosinase (SA_ty) (5 U) was added to initiate hydrogel crosslinking, and the cell-laden hydrogel mixture was immediately transferred to 24 well plates. Culture media was added to provide the nutrient for the cells and live cell imaging was performed using an NIR fluorescence microscope for up to 2 weeks. The number of viable cells was counted at each time point based on the fluorescence signal of the cells in the 700 nm channel (**Figure 3A**). The total area of the cells was calculated based on the FL signal and divided by the area of a single cell to determine the number of proliferated cells at each time point. Cells embedded in 1% NIR-gelatin had steady proliferation rate (**Figure S4**); however, cells embedded in 3% NIR-gelatin stopped proliferating 3-d post-incubation, and most of the cells were dead and the fluorophores inside the cells eluted to the

nearby hydrogel by 8-d post-incubation (**Figure S5**). Next, we quantified and plotted signal intensity changes in both the cells and NIR hydrogel in 700 and 800 nm channels, respectively (**Figure 3B**). We observed a gradual intensity decrease of the cells over time, as an indication of active proliferation in 1% NIR-gelatin. When the cells proliferate, the number of fluorophores that are uptaken gets divided between the mother and daughter cells. We also saw a gradual decrease in the intensity of NIR hydrogel as it degraded.

In vivo physiological stability and degradation of NIR hydrogels

To investigate the optical- and bio-stability of ZW800-3a after its conjugation with the hydrogel, we performed a real-time non-invasive longitudinal monitoring of the hydrogel in nude mice for up to 3 weeks. NIR hydrogel (100 µL) was injected into subcutaneous of the flank region of nude mice and NIR signal was quantified and plotted every 3-5 d. (**Figure 3C-D**). Shrinkage of the hydrogel was observed after initial swelling. Previously, different groups have attempted to label hydrogel with commercially available fluorophores (e.g., Alexa488) that have lower excitation and emission wavelength [32]. These fluorophores are not stable enough to track the hydrogel for an extended period of time because of *in vivo* instability from biological enzyme attacks, resulting loss of fluorescence before the actual degradation of the hydrogel. In addition, we believe covalent conjugation of the fluorophore prevented staining nearby tissue, minimizing false margin of the implanted hydrogel. We confirmed this by removing the skin and observed the fluorescence signal only in the hydrogel (**Figure S6A**). The composition of NIR hydrogel is degradable by endogenous hyaluronidase. We consequently traced degraded hydrogel on 21-d post-injection, and most of them were found in the intestine, suggesting hepatobiliary clearance of disassembled hydrogel (**Figure S6B**).

Multichannel imaging of hydrogel degradation and tissue growth

Dual-channel fluorescence imaging strategy is used to track host tissue growth and scaffold degradation after brain implantation. Twenty microliters of NIR hydrogel was intracranially injected into the brain of animals by the defined coordinates on stereotactic. Ox1 (100 nmol) was intravenously administered into the same animals an hour before NIR imaging time points. Images of the whole and sectioned brain tissues were acquired in 700 nm (red) and 800 nm (green) channels simultaneously, followed by merging into colocalize ingrowth area over the implanted scaffold (**Figure 4A**). We also performed *in vivo* dual-channel imaging to show fluorescence signal of the NIR hydrogel transplanted brain through the intact skull and after skull removal 7-d post-implantation (**Figure S7**).

After brain damage, limited blood supply due to the damaged vasculature with increases inflammatory and immune response prevents the delivery Ox1 to the damaged area [33]. We observed high scaffold signal on 1-d and 7-d post-implantation and no significant signs of tissue growth within the hydrogel, whereas substantial decreased signal was observed in the scaffold on 14-d post-implantation. In the merged images, the area where tissue increased tissue growth has mixture of red and green color resulting light green to orange.

In addition, we imaged the whole brain to diagnose any abnormal signs of intracerebral pressure build up or prevention of normal vasculature blood flow in the consequence of injecting high volume of hydrogels. We observed limited blood supply from the circulation 1-d post-injection of the hydrogel of the transplanted side of the whole brain (**Figure S8A**). Interestingly, the full blood flow to the brain was recovered by 7-d post-implantation. The quick recovery of blood flow in the brain suggests the NIR hydrogel did not cause vasculature damage to the host tissue as the formulation of the hydrogel allow minimal invasiveness for the delivery and fast situ gelation prevented the large diffusion of the biomaterial into parenchyma. We also observed migration of degraded hydrogels in all directions to the nearby tissue in the 800 nm single channel with increased distance from the injection site with prolonged implantation period (**Figure S8B**). However, we were not able to trace disassembled hydrogel in the other parts of the body such as spinal cord, choroid plexus, brain stems, etc. The advantages of using optical imaging are high sensitivity and spatial resolution, which have the ability to obtain structure and physiological information. From the acquired images, we developed a quantification method to accurately calculate the percentage of ingrown tissue within the hydrogel.

Quantitative annotation of brain tissue ingrowth

Image segmentation is used in the medical field to provide precise analytical information. It utilizes segmentation by labeling every pixel in an image where similar characteristics are assigned with the same label. We applied this method to quantify and annotate the regenerated tissue based on the FL intensity in the therapeutic region where hydrogel has been implanted (**Figure 4B**). Three segmented binary

images were generated by setting the lower and upper threshold value based on the histogram intensity of Ox1 (700 nm) at each time point. These binary images were then color-coded, merged, and reconstructed to provide dynamic color mapping to show clear boundaries within the therapeutic area. For quantitative analysis, the number of pixels in each color were calculated to determine the overall percentage of proliferation (yellow), active expansion (magenta), and the resting (cyan) area (**Figure 5A**). With our multispectral imaging system and quantification method, we can localize the damaged area with limited tissue growth (resting area) after the initial treatment and can be used provide a next treatment plan.

Histological analysis using NIR fluorescence microscopy

Tissue ingrowth and scaffold degradation were evaluated at a microscopic level by collecting brain samples after the dual-channel imaging. Hematoxylin and eosin (H&E) staining was performed on the samples cut at 10 µm and observed through NIR fluorescence microscope (**Figure 5B**). The microporous structure of hydrogel was observed 1-d post-implantation and was well maintained up to 21-d in the degradation process. We found a reduction in the fluorescence signal intensity and the decrease in the thickness of hydrogel after the initial swelling. Cell infiltration and adhesion around the hydrogel were observed 7-d post-implantation, indicating rapid cellular infiltrations without the need for bulk degradation. The cells continue to infiltrate and proliferate within the hydrogel, expanding the ingrowth area by 14-d and even more on 21-d post-implantation. These histological evaluations were consistent with *in vivo* fluorescence images. Therefore, a combination of *in vivo* imaging and histological analysis can provide substantial information needed to determine the regeneration capacity of the implanted scaffold. Alternatively, this technique can be combined with fluorescence protein expressing cells to monitor *in vivo* behavior of transplanted cells within the hydrogel.

Conclusions

In this study, we have developed a novel dual-channel optical imaging technique to simultaneously track scaffold degradation and brain tissue ingrowth over the complete regeneration period. High-resolution imaging with multispectral capability will be further useful to localize and quantify brain tissue growth and to monitor the therapeutic efficacy of scaffold in the brain. NIR-II

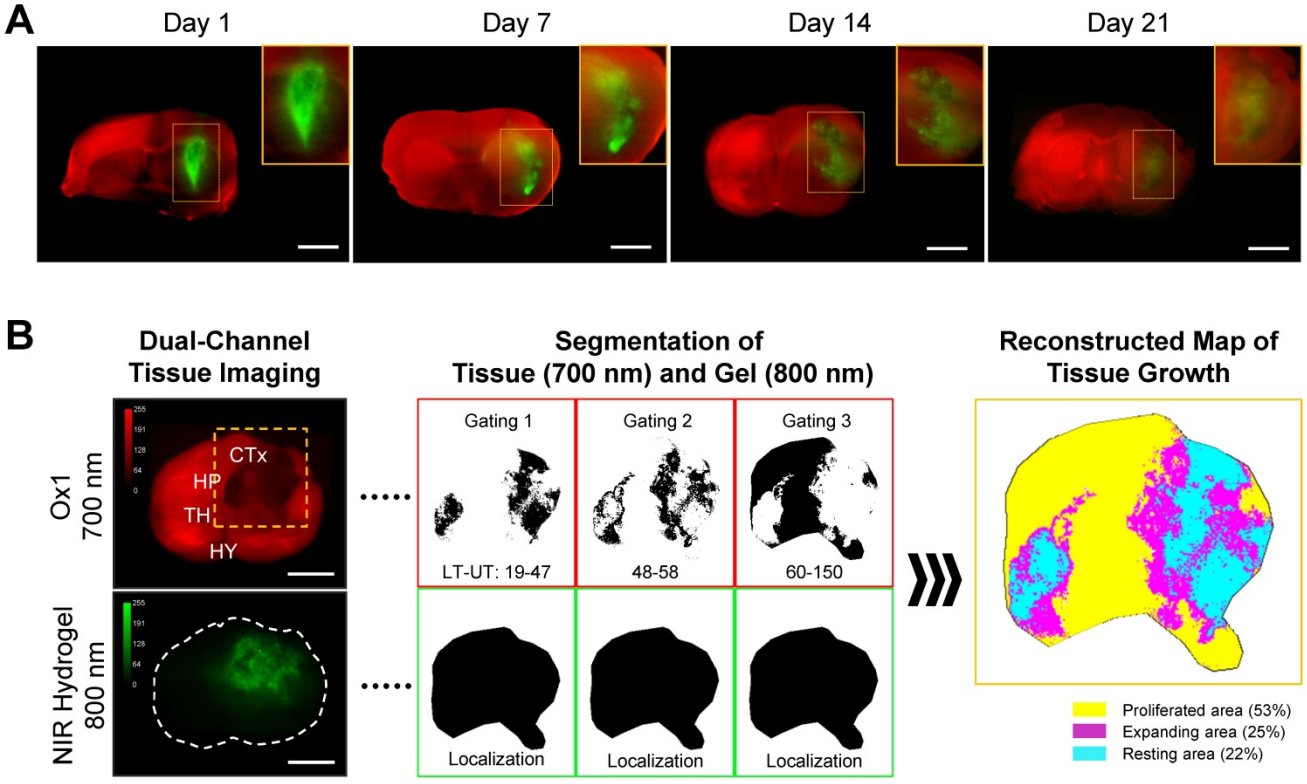

Figure 4. Dual-channel imaging of brain tissue growth and NIR hydrogel. (A) NIR hydrogel (20 µL) was injected into the brain of animals and Ox1 (100 nmol) was administered to the same animal an hour prior to the dual-channel imaging. Brain tissue ingrowth (red) and NIR hydrogel (green) degradation observed in the merged image. Sample thickness = 2 mm. **(B)** Spatial segmentation analysis of the NIR image for the quantification and visualized dynamic color mapping of the tissue ingrowth. Scale bars = 2.5 mm.

imaging window will be absolutely beneficial for this application, and we believe that our multispectral optical imaging technique could play a significant role in translating regenerative medicine to the clinic with an aim to provide a high quality of life to patients and their families after recovering from devastating brain diseases.

Materials and Methods

NIR fluorophores and hydrogels. Type A gelatin (40 – 50 kDa) from porcine skin, Oxazine1 (Ox1), and tyramine hydrochloride were purchased from Sigma-Aldrich (St. Louis, MO), and hyaluronic acid (40 – 60 kDa) were from Lifecore Biomedical (Chaska, MN). ZW800-3a was synthesized as previously reported [20] and used for conjugation with the gelatin via the EDC/NHS coupling chemistry. Briefly, 7.86 mg of ZW800-3a was added to 1 mL of distilled water containing 9.585 mg of EDC, and 10.85 mg of sulfo-NHS and shaken at room temperature for 30 min. Gelatin (1 wt%) was dissolved in 20 mL of distilled water at 60 °C and pH was adjusted to 8.5 by adding NaOH. After gelatin has completely dissolved, pre-activated ZW800-3a NHS ester was slowly added and then the mixture was shaken for 1 h. Unconjugated dyes were filtered using dialysis and the final product was lyophilized. To prepare hyaluronic acid-tyramine conjugate (HA-ty), 1.437 g of EDC, 0.863 g of NHS and 1.302 g of tyramine were added to 1.0 g of HA sodium salt dissolved in 100 mL of distilled water. Unconjugated tyramine was filtered using dialysis and HA-ty was collected after lyophilization. The final product was analyzed by NMR and UV spectroscopy and 33% of degree tyramine substitution was confirmed.

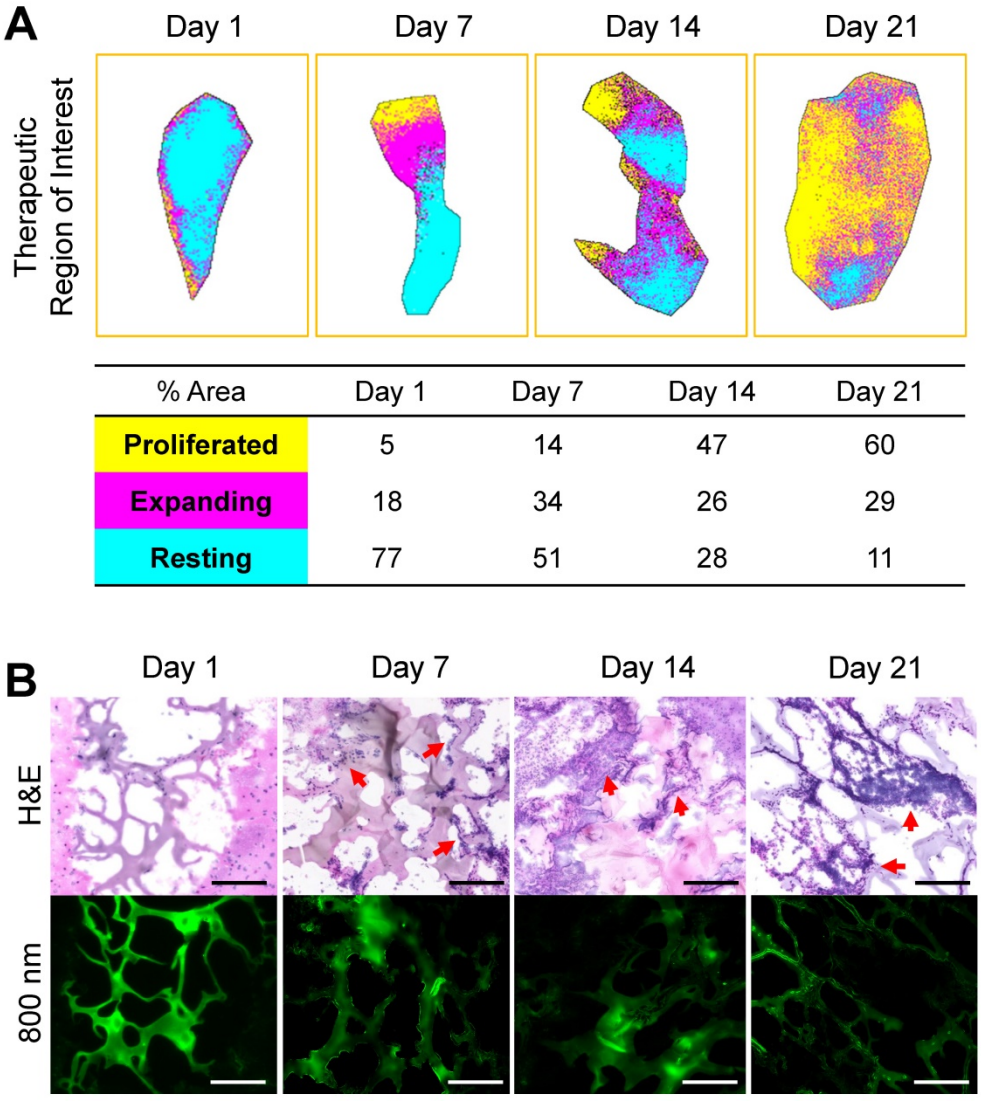

% Area	Day 1	Day 7	Day 14	Day 21
Proliferated	5	14	47	60
Expanding	18	34	26	29
Resting	77	51	28	11

Figure 5. Reconstructed map of tissue ingrowth and histological analysis at each time point. (A) Time course *in vivo* localization and quantification of brain tissue growth within the therapeutic region of implanted hydrogel. **(B)** H&E and NIR imaging of scaffold from the brain samples collected at 1-, 7-, 14-, and 21-d post-implantation of the hydrogel. Sample thickness = 10 µm. Scale bars = 50 µm.

Optical property measurements. Absorbance and fluorescence were measured using fiber optic HR2000 (200-1100 nm) spectrometers by a 5 mW, 655 nm laser diode (Opcom Inc, Xiamem, China) coupled through a 300 mm core diameter. NA 0.22 fiber (Fiberguide Industries, Stirling, NJ). 5 x 10^{-6} M of each fluorophore solution was prepared in 10% fetal bovine serum (FBS) in PBS. In silico calculations of physiochemical properties such as molecular weight, charge distribution, log*D* at pH 7.4, pKa, rotatable bonds were calculated using JChem calculator plugins (ChemAxon, Budapest, Hungary). Data was plotted using Prism7 software (GraphPad, San Diego, CA) and Microsoft Excel (Redmond, WA).

Analysis of mechanical properties. The Young's modulus of hydrogel was evaluated by Ultimate Testing Machine (UTM, 100N of the load cell, EZ-SX STD, Shimadzu, Japan). Briefly, the hydrogel was crosslinked overnight into customized PDMS mold (diameter: 8 mm, thickness: 2 mm). Then, the samples were loaded on the holder and performed the test with 0.5 mm/min of the probe speed. The Young's modulus was calculated in the range of strain from 5% to 15%. All the experiments were triplicate.

Rheological analysis. The viscoelastic properties of hydrogel were evaluated in Anton Paar Demo Lab using rheometer (MCR 302, Measuring cell: P-PTD & H-PTD 200, Measuring System: pp25, Anton-Paar, Austria). All the samples were prepared in PDMS mold (diameter: 8 mm, thickness: 2 mm). At first, we conducted frequency sweep. Briefly, the sample was loaded on the plate, and detection probe was positioned on the sample with 2 mm gap. The G' and G" was measured according to variation of frequency from 1 to 100 Hz. In frequency sweep, the strain was fixed at 1%. To evaluate a critical strain, we checked the viscoelastic properties with increasing strain from 0.1 to 500%.

Live cell labeling and tracking in the NIR hydrogel. C2C12, mouse myoblast cells, was cultured with DMEM/F12, supplemented with 10% FBS and 1% P/S and incubated at 37 ^{o}C in a humidified 5% CO_2 incubator. When cells reached 80-90% confluence, the seeded cells were rinsed twice with PBS and ESNF13 (cell tracking NIR fluorophore) was added at a concentration of 5 μM and incubated for 20 min at 37 ^{o}C. Cells were washed three times with PBS and detached with trypsin and centrifuged and the supernatant was removed. These cells were then embedded in the mixture of 1wt% HA and 1 or 3wt% NIR-gel and SA_ty was added to five a final density of 4 x 10^5 cells/mL and then 100 μL was transferred to a 24-well plate. After 30 min incubation in 37 ^{o}C, culture media was added to provide nutrients to the cells. The cells and hydrogel were observed for 12-d under the 4-channel TE2000 NIR fluorescence microscope. Two custom filter (Chroma Technology Corporation, Brattleboro, VT) composed of 650 ± 22 nm and 750 ± 25 nm excitation filter, 675 nm and 785 nm dichroic mirrors, and 710 ± 25 nm and 810 ± 20 nm emission filters were used to detect cells and NIR hydrogel, respectively. Fluorescent intensity (FI) of region of interest (ROI) was quantified using image J software (NIH, Bethesda, MD). Results were presented as mean ± standard deviation (s.d.).

***In vitro* cell viability test.** The number of viable cells was counted at each time point by separating the fluorescence (FL) signal of the cells from the background. To separate the FL signal of cells, we first converted the images to binary format using Image J software (NIH, Bethesda, MD). The total FL area was then calculated and divided by the average area of single cell to determine the number of cells. The proliferated cells were quantified by comparing the number of mother cells and daughter cells using Image J software.

Animal models for hydrogel implantation. All animal studies were performed under the supervision of MGH IACUC and housed in an AAALAC certified facility with approved protocol #2016N000622. C57BL/6 mice (8 weeks) and NCRNU nude mice (20-30 g, 6-8 weeks) were purchased from Jackson Laboratory and Taconic Farms, respectively. Mice were anesthetized with an intraperitoneal injection of ketamine (100 mg/kg) and xylazine (10 mg/kg). Nude mice were used for subcutaneous implantation of the NIR hydrogel. 100 μL of NIR hydrogel were injected into each side of the flank (n = 3). Noninvasive optical imaging was performed from the same animal every week for 3 weeks using the K-FLARE imaging system.

Optical fluorescence imaging system and quantification. For dual-NIR channel imaging, 1 mW/cm^2 of a 660-nm excitation light (NIR #1) and 3.6 mW/cm^2 of a 760-nm excitation light (NIR #2) were used with white light (400-650 nm) at 5,500 lux. Simultaneous color images (512 × 512 pixels) with the choice of either 700 nm or 800 nm fluorescence images were acquired using an AD-130GE camera (JAI, Yokohama, Japan) installed with custom dual bandpass prism (channel 1: 710/50, channel 2: 780lp). The imaging system was remotely controlled by custom software at rates up to 15 Hz, except for field of view that was manually adjusted by a 3CCD zoom lens (Goyo Optical Inc., Saitama, Japan). In the color-NIR merged image, 700-nm fluorescence and 800-nm fluorescence were pseudo-colored red and green, respectively. The imaging head was positioned at a distance of 9 in from the surgical field, and all NIR

fluorescence images have identical exposure times and normalizations.

Intracranial transplantation of NIR hydrogel and brain tissue imaging. C57BL/6 mice were used for intracranial transplantation. 20 μL of NIR hydrogel was injected using a 28-gaugue needle with the following coordinates: anterior-posterior = 1 mm, medial-lateral = 2 mm, and dorsal-ventral = 2.5 mm. Animals were injected with 100 nmol of Ox1 intravenously 1 h prior to imaging on each day (1-, 7-, 14-, and 28-d post-transplantation). After intraoperative imaging, animals were sacrificed, and each brain was extracted for dual-channel imaging. Whole brain images were taken first, and then the brain was cut consecutively with a 2 mm thickness in coronal sections. Hydrogel-injected brain sections were imaged simultaneously at 700 nm (NIR #1) and 800 nm (NIR #2) channels at various exposure times.

Histological analysis and NIR fluorescence microscopy. NIR hydrogel-injected brain samples were mounted in Tissue-Teck OCT compound (Fisher Scientific, Pittsburgh, PA) and flash-frozen in liquid nitrogen. These samples were cut to a 10 μm thickness and stained with hematoxylin and eosin (H&E) and fluorescence microscopy was performed to acquire images. NIR fluorescence microscopy was performed on TE2000 described above.

Supplementary Material

Supplementary figures.
http://www.thno.org/v09p4255s1.pdf

Acknowledgements

This research was supported by the US NIH grant NIBIB #R01EB022230, NHLBI #R01HL143020, and NCI #R21CA223270. This work was also supported by the National Research Foundation of Korea Grant (NRF-2017K1A3A1A19070731, NRF-2017 M3A9C6031786, NRF-2016R1E1A1A01943393, and NRF-2019M3A9G1023840). The Institute of Engineering Research at Seoul National University provided research facilities for this work.

Author contributions

GKP, HSC, and NSH designed research; GKP, SHK, KMK, and PD performed the experiments; GKP wrote the manuscript. HSC and NSH supervised and finalized the manuscript.

Competing Interests

The authors have declared that no competing interest exists.

References

1. Maas AI, Stocchetti N, Bullock R. Moderate and severe traumatic brain injury in adults. Lancet Neurol. 2008; 7: 728-41.
2. Ward NS. Restoring brain function after stroke - bridging the gap between animals and humans. Nat Rev Neurol. 2017; 13: 244-55.
3. Bond AM, Ming GL, Song H. Adult Mammalian Neural Stem Cells and Neurogenesis: Five Decades Later. Cell Stem Cell. 2015; 17: 385-95.
4. Lane SW, Williams DA, Watt FM. Modulating the stem cell niche for tissue regeneration. Nat Biotechnol. 2014; 32: 795-803.
5. Nih LR, Gojgini S, Carmichael ST, Segura T. Dual-function injectable angiogenic biomaterial for the repair of brain tissue following stroke. Nat Mater. 2018; 17: 642-51.
6. Nih LR, Carmichael ST, Segura T. Hydrogels for brain repair after stroke: an emerging treatment option. Curr Opin Biotechnol. 2016; 40: 155-63.
7. Park KM, Park KD. In Situ Cross-Linkable Hydrogels as a Dynamic Matrix for Tissue Regenerative Medicine. Tissue Eng Regen Med. 2018; 15: 547-57.
8. Park KJ, Jeon TY, Yoo SY, Kim JH, Eo H, Song KD. The appearance of dextranomer-hyaluronic acid copolymer implants on ultrasound may predict resolution of vesicoureteral reflux after injection therapy. Clin Radiol. 2014; 69: 939-44.
9. Kim KS, Kim YS, Bao K, Wada H, Choi HS, Hahn SK. Bioimaging of botulinum toxin and hyaluronate hydrogels using zwitterionic near-infrared fluorophores. Biomater Res. 2017; 21: 15.
10. Park GK, Hoseok s, Kim GS, Hwang NS, Choi HS. Optical spectroscopic imaging for cell therapy and tissue engineering. Appl Spectrosc Rev. 2018; 53: 360-75.
11. Park GK, Lee JH, Levitz A, El Fakhri G, Hwang NS, Henary M, et al. Lysosome-Targeted Bioprobes for Sequential Cell Tracking from Macroscopic to Microscopic Scales. Adv Mater. 2019; 31: 1806216.
12. Kim SH, Lee JH, Hyun H, Ashitate Y, Park G, Robichaud K, et al. Near-infrared fluorescence imaging for noninvasive trafficking of scaffold degradation. Sci Rep. 2013; 3: 1198.
13. Artzi N, Oliva N, Puron C, Shitreet S, Artzi S, bon Ramos A, et al. In vivo and in vitro tracking of erosion in biodegradable materials using non-invasive fluorescence imaging. Nat Mater. 2011; 10: 704-9.
14. Kim SH, Lee HR, Yu SJ, Han ME, Lee DY, Kim SY, et al. Hydrogel-laden paper scaffold system for origami-based tissue engineering. Proc Natl Acad Sci U S A. 2015; 112: 15426-31.
15. Gomes ME, Rodrigues MT, Domingues RMA, Reis RL. Tissue Engineering and Regenerative Medicine: New Trends and Directions-A Year in Review. Tissue Eng Part B Rev. 2017; 23: 211-24.
16. Choi HS, Gibbs SL, Lee JH, Kim SH, Ashitate Y, Liu F, et al. Targeted zwitterionic near-infrared fluorophores for improved optical imaging. Nat Biotechnol. 2013; 31: 148-53.
17. Zhu S, Yung BC, Chandra S, Niu G, Antaris AL, Chen X. Near-Infrared-II (NIR-II) Bioimaging via Off-Peak NIR-I Fluorescence Emission. Theranostics. 2018; 8: 4141-51.
18. Zhu S, Tian R, Antaris AL, Chen X, Dai H. Near-Infrared-II Molecular Dyes for Cancer Imaging and Surgery. Adv Mater. 2019: 1900321.
19. Hyun H, Owens EA, Narayana L, Wada H, Gravier J, Bao K, et al. Central C-C Bonding Increases Optical and Chemical Stability of NIR Fluorophores. RSC Adv. 2014; 4: 58762-8.
20. Choi HS, Nasr K, Alyabyev S, Feith D, Lee JH, Kim SH, et al. Synthesis and in vivo fate of zwitterionic near-infrared fluorophores. Angew Chem Int Ed Engl. 2011; 50: 6258-63.
21. Hou S, Xu Q, Tian W, Cui F, Cai Q, Ma J, et al. The repair of brain lesion by implantation of hyaluronic acid hydrogels modified with laminin. J Neurosci Methods. 2005; 148: 60-70.
22. Kim SH, Lee SH, Lee JE, Park SJ, Kim K, Kim IS, et al. Tissue adhesive, rapid forming, and sprayable ECM hydrogel via recombinant tyrosinase crosslinking. Biomaterials. 2018; 178: 401-12.
23. Pandey BP, Lee N, Kim BG. Effect of Extracellular Tyrosinase on the Expression Level of P450, Fpr, and Fdx and Ortho-hydroxylation of Daidzein in Streptomyces avermitilis. Appl Biochem Biotechnol. 2018; 184: 1036-46.
24. Hintersteiner M, Enz A, Frey P, Jaton AL, Kinzy W, Kneuer R, et al. In vivo detection of amyloid-beta deposits by near-infrared imaging using an oxazine-derivative probe. Nat Biotechnol. 2005; 23: 577-83.
25. Leipzig ND, Shoichet MS. The effect of substrate stiffness on adult neural stem cell behavior. Biomaterials. 2009; 30: 6867-78.
26. Massensini AR, Ghuman H, Saldin LT, Medberry CJ, Keane TJ, Nicholls FJ, et al. Concentration-dependent rheological properties of ECM hydrogel for intracerebral delivery to a stroke cavity. Acta Biomater. 2015; 27: 116-30.
27. Rashid B, Destrade M, Gilchrist MD. Mechanical characterization of brain tissue in compression at dynamic strain rates. J Mech Behav Biomed Mater. 2012; 10: 23-38.
28. Taylor Z, Miller K. Reassessment of brain elasticity for analysis of biomechanisms of hydrocephalus. J Biomech. 2004; 37: 1263-9.
29. Budday S, Nay R, de Rooij R, Steinmann P, Wyrobek T, Ovaert TC, et al. Mechanical properties of gray and white matter brain tissue by indentation. J Mech Behav Biomed Mater. 2015; 46: 318-30.
30. Antonovaite N, Beekmans SV, Hol EM, Wadman WJ, Iannuzzi D. Regional variations in stiffness in live mouse brain tissue determined by depth-controlled indentation mapping. Sci Rep. 2018; 8: 12517.
31. Kim SH, Park G, Hyun H, Lee JH, Ashitate Y, Choi J, et al. Near-infrared lipophilic fluorophores for tracing tissue growth. Biomed Mater. 2013; 8: 014110.

32. Liang Y, Bar-Shir A, Song X, Gilad AA, Walczak P, Bulte JW. Label-free imaging of gelatin-containing hydrogel scaffolds. Biomaterials. 2015; 42: 144-50.
33. Aktas O, Ullrich O, Infante-Duarte C, Nitsch R, Zipp F. Neuronal damage in brain inflammation. Arch Neurol. 2007; 64: 185-9.